ELSEVIER

Ceramics International 29 (2003) 735–744

CERAMICS INTERNATIONAL

www.elsevier.com/locate/ceramint

Processing, microstructure and mechanical strength of reaction-bonded Al_2O_3 ceramics

Sébastien Bertrand[a,1], Thibaut Michalet, Agnès Giraud, Michel Parlier[a,*], Alain Bataille[b], Richard Duclos[b], Jacques Crampon[b,*]

[a]*Office National d'Etudes et de Recherches Aérospatiales, DMSC, 29 Avenue Division Leclerc, BP72, 92320 Châtillon, France*
[b]*Laboratoire de Structure et Propriétés de l'Etat Solide, ESA-CNRS 8008, Université des Sciences et Technologies de Lille, Bât C6, 59655 Villeneuve d'Ascq, France*

Received 18 February 2002; received in revised form 3 March 2002; accepted 10 November 2002

Abstract

Reaction-bonded Al_2O_3 (RBAO) ceramics were fabricated from attrition-milled Al/Al_2O_3 powder mixtures. Two different Al precursor powders and several contents of Al were used. The raw materials and the RBAO powder mixtures were studied in terms of grain size, oxidation behaviour (TGA/DTA), morphology and microstructure. The influence of the important parameters controlling the RBAO process is first discussed. Secondly, the microstructure of RBAO bodies uniaxially pressed and heat-treated in air, up to 1100 and 1250 °C, is reported and their mechanical strength is evaluated and compared to conventional Al_2O_3 ceramics.

Keywords: A. Milling; A. Sintering; C. Strength; D. Al_2O_3

1. Introduction

As an alternative to conventional ceramic processing, reaction-bonded ceramics (RBC) offer attractive attributes such as: *(i)* particularly low-shrinkage during sintering, *(ii)* low processing temperature, *(iii)* low raw material cost and near-net-shape tailorability [1,2]. Indeed, high linear shrinkage (~15%) is usually associated with the conventional sintering of ceramic powders, whereas RBC ceramics are characterised by low-to-zero shrinkage capability. RBC are usually fabricated from metallic powder compacts, which are converted to ceramics by reaction with a gaseous phase prior to, or during sintering. That's the reason why this process has been most intensively studied in non-oxide systems, such as reaction-bonded silicon nitride (RBSN) and reaction-bonded silicon carbide (RBSC) [3], and is now also successfully applied in oxide systems, such as reaction-bonded aluminium oxide (RBAO) [4] and reaction-bonded mullite (RBM) [5].

The oxidation of aluminium, in an Al/Al_2O_3 powder mixture, forms an alumina compact with small dimension changes between the green and the reaction-bonded state [4]. The steps of the RBAO process [6–9] mainly consist of: *(i)* attrition milling of the precursor powders (Al/Al_2O_3 powder mixtures, with typically, 30–60 Al vol.%) to reduce the powder mixture grain size and because high-strength alumina requires fine and homogeneous powders [7], and then *(ii)* heat-treatment in air. During this last step, the volume expansion ($\Delta V/Vo \sim 28\%$), associated with the Al to α-Al_2O_3 transformation, partially compensates for the sintering shrinkage. This RBAO process can be modified by incorporating metal or ceramic additives (such as Zr, Ti, Cr, Nb or ZrO_2, SiC) in order to change the composition, to accelerate the reaction, to further compensate for the sintering shrinkage and to improve the mechanical properties respectively [5,6,10–13]. Numerous authors have studied the RBAO process in terms of reaction mechanisms, microstructure and mechanical properties, to define the advantages and the drawbacks

* Corresponding authors.
E-mail addresses: parlier@onera.fr (M. Parlier), jacques.crampon@univ-lille1.fr (J. Crampon).
[1] Present address: SNECMA-Moteurs, Rocket Engine Division, Solid Propulsion and Composites Direction, Les Cinq Chemins, 33187 Le Haillan, France.

0272-8842/03/$30.00
doi:10.1016/S0272-8842(02)00225-0

of the method. For the mechanical properties, it can be noticed that the majority of the previous studies, have been achieved on RBAO ceramics with additives, or with a post-HIP treatment [14,15].

In the present work, we report the processing of RBAO, sintered at relatively low temperatures. Different raw materials have been studied and milled in several conditions. The relationship of the RBAO processing parameters, microstructure and mechanical strengths of the sintered ceramics was then investigated.

2. Experimental procedure

In order to investigate the influence of the particle size and morphology of the aluminium powder on the milling and on the reaction-bonding behaviour two types of commercially available Al powders were used in the present study: Al_C flakes (Cerac, WI, USA, A-1183) with a mean size of 1.6 μm, and Al_E globular particles (Eckart-Poudmet, France) with an average size of 4.6 μm, together with a fine alumina powder (0.9 μm) (Baikowski, France, Baikalox-CR1, 500 ppm doped-MgO). The morphology of the powders is presented in Fig. 1.

Table 1
Specific area of aluminium and impurity content of aluminium and alumina

	Specific area (m^2/g)	Impurity content (wt)			
		Fe	Si	K	Na
Al_C	6.98	0.2%	0.1%	–	–
Al_E	1.2	<0.2%	<0.1%	–	–
Al_2O_3		6 ppm	31 ppm	19 ppm	6 ppm

The impurity content of the powders and the specific area of the Al powders are listed in Table 1. The nominal compositions of the Al/Al_2O_3 powder mixtures studied in the present work are listed in Table 2.

The powder mixtures were attrition milled (Union process, Ohio, USA) in 2-propanol as the milling fluid, using a polymeric vessel filled with 10 wt.% powder mixture and 90 wt.% ZrO_2 milling balls. The attrition milling intensity was varied by changing the milling time. Before the granulometric analysis (Horiba CAPA-700, Japan), the powders were de-agglomerated and the mixture was homogenised by ultrasound for 15 min.

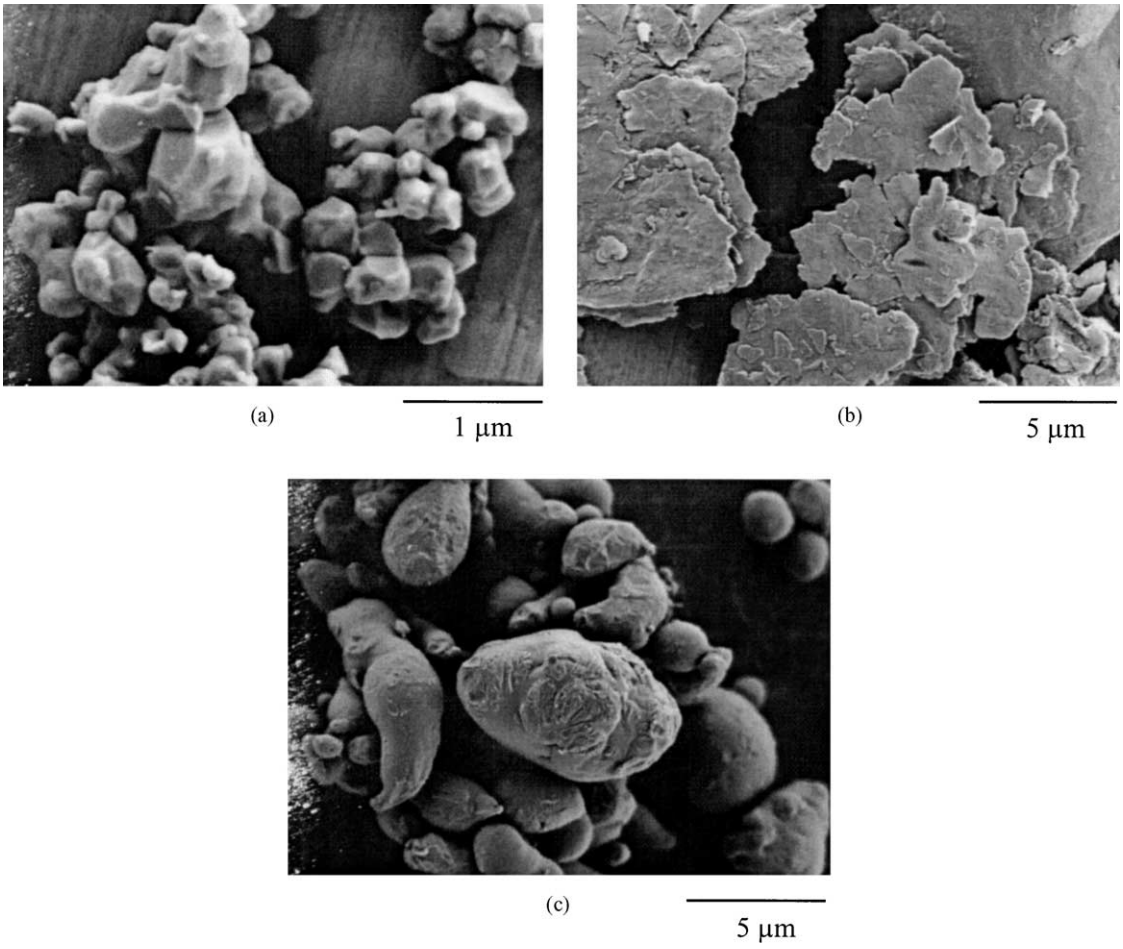

Fig. 1. SEM of the powders used in the present work: (a) Al_2O_3 powder, (b) Al_C flakes powder and (c) Al_E globular powder.

Table 2
Powder mixtures

Batch	Composition (vol.%)	Mean size (μm)	Milling time (h)	Amount of Al oxidised (vol.%)	d_{50} (μm)
#1	Al_C (40)–Al_2O_3 (60)	1.2	–	6	1.2
#2	Al_C (40)–Al_2O_3 (60)	1.2	24	31	0.3
#3	Al_C (80)–Al_2O_3 (20)	1.5	8	12	0.5
#4	Al_E (60)–Al_2O_3 (40)	3.1	8	49	0.9
#5	Al_E (80)–Al_2O_3 (20)	3.9	8	8	1.8
#6	Al_E (80)–Al_2O_3 (20)	3.9	28	26	0.9

The milled powders were characterised in terms of, microstructure (Scanning Electron Microscopy, SEM, LEO DSM 982 Gemini) and thermogravimetric analysis (TGA, Setaram, TG92-16). The dilatometric study (DI 20, Adamel Lhomargy, France), was performed in air at temperatures up to 1300 °C, on discs of diameter 12.8 mm and thickness 2 mm, obtained from dried and uniaxially pressed ($\sigma \sim 300$ MPa) powders. The density of the green samples was geometrically estimated, whereas those of the sintered discs was measured by the Archimedes water displacement method.

To obtain three-point bending samples, the dried powder mixtures were uniaxially pressed at $\sigma \sim 300$ MPa to form rectangular-section bars of 40 mm×16 mm×2.2 mm. These compacts were then reaction-bonded, using a heating cycle deduced from the TGA experiments, and sintered in air at two different temperatures: 1100 and 1250 °C in function of the desired porosity.

The microstructure of the porous RBAO samples sintered at 1100 °C and 1250 °C was observed by SEM from fracture surfaces of the three point bending samples. Bending strength values of polished samples was measured in the air by the three-point loading method, using rectangular bars with dimensions of 2 mm×4.5 mm×35 mm (using 30 mm measuring span) and a cross-head velocity of 0.3 mm min^{-1}. For each material type, the average data obtained from five specimens were used for the subsequent analysis.

3. Results and discussion

3.1. Powder mixture processing

The important parameters, which determine the quality of the Al/Al_2O_3 mixture are the volume ratio of the powder mixture to the grinding medium and the milling time. The first parameter has been chosen on the basis of a previous study [7] into the optimum range 0.05–0.2. Numerous milling experiments were performed to check the second parameter. The main object of the powder conditioning was to find milling conditions which produce fine and homogeneous powder mixtures without oxidising too much the Al particles. The results of TGA measurements used to evaluate the amount of Al oxidised during milling of the powder mixtures (noted V_{Al}) are listed in Table 2. In all the attrition-milled mixtures, between 8% and 49% of the initial amount of Al in mixtures is oxidised after the milling process.

The particle-size distributions obtained on the milled powder mixtures are presented in Fig. 2. The medium particle size (d_{50}) of the Al/Al_2O_3 milled powder mixtures is compared in Table 2 to mean particle size of the initial RBAO powder mixtures, before milling attrition, which is determined from a law of mixture according to the mean particle size of the raw materials. The agreement between the experiment ($d_{50} = 1.2$ μm) and the mixture law is very good for the batch #1 because there is only a mixing process and no milling attrition for this batch. By the comparison of the batch #5 with the batches #4 and 6, it is observed that Al particle size decreases with the increase of the content of the Al_2O_3 particles and with the increase of the milling time. Furthermore, a pseudo plateau-like domain was attained when the milling time was prolonged e.g. between 14 h and 28 h. Generally, milling time of 8 h was sufficient to reduce Al mean particle size to <1 μm, except for the Al powder mixture of the batches #5 and #6. For the corresponding mixture, the content of the Al_2O_3 abrasive particles is so low (20 vol.%) that it requires a milling time >14 h to obtain a particle size <1 μm. For the batch #2, the medium particle size after attrition milling ($d_{50} = 0.3$ μm) is below that of the fine Al_2O_3 powder (0.9 μm). This corresponds certainly to a de-agglomeration and/or a crushing of the Al_2O_3 milled powder.

The complexity of the powder mixture morphology is illustrated in Fig. 3 showing SEM micrographs of the milled powder mixtures. After attrition-milling, depending on the Al/Al_2O_3 volume ratio (80/20 for batches #3, 5, 6; 60/40 for batch #4; and 40/60 for batch #2) and on the used milling time, the two types of precursor powders tend to exhibit less different morphologies. When a small amount of Al_2O_3 powder (20 vol.%) was mixed and attrition milled with Al powder for a short time (8 h) flake shapes were retained in the powder mixture (batches #3 and 5) as shown in Fig. 3. However, the cutting effect of the milling media was effective in batch #3 and some fragmentation of the Al_c flakes occurred and their size was reduced. When Al_E globular powder was used (batch #5), a similar flaky microstructure was developed. In this batch, the Al_E globular particles begin to be laminated into flakes by the plastic deformation induced by the milling action. The fragmentation of the Al_E globular particles increases after a long milling time (28 h, batch #6) and the powder mixture exhibits now similar morphology and particle size to that observed in the batch #4. The comminution of the Al particles increases also strongly with

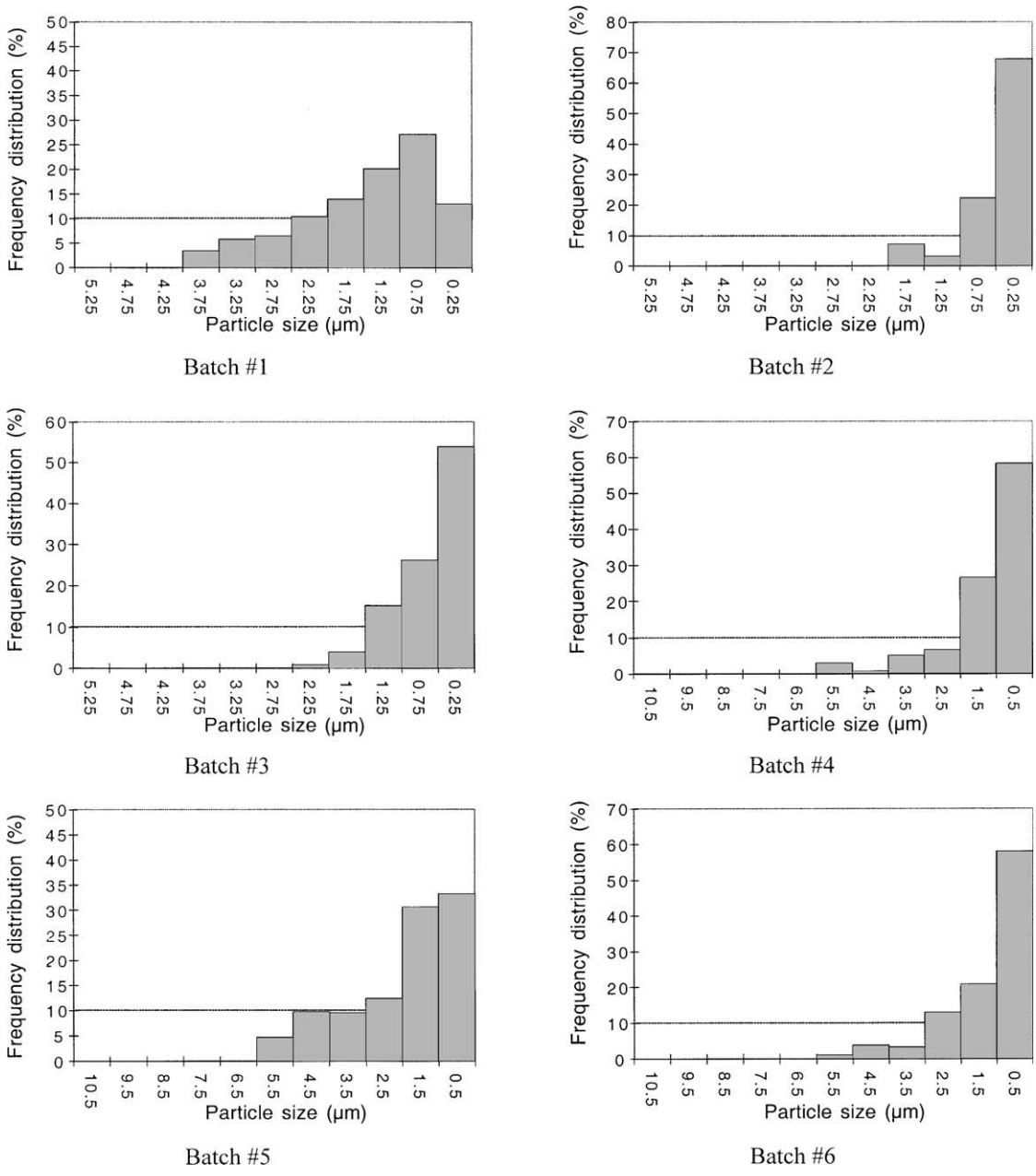

Fig. 2. Particle-size distribution of the milled powder mixtures.

the content of the hard Al_2O_3 particles which assist the plastic deformation and the fragmentation of the Al particles [9] (batches #4 and #2). In the batch #2, the long attrition-milling time (24 h) has been efficient to reduce strongly the size and the flake shape of the Al_c particles.

3.2. Heat treatment

The TGA curves, up to 1400 °C, show that the two aluminium raw powders present different oxidation behaviours (Fig. 4a). The maximum relative weight gains are 0.72 (0.78 when corrected by the initial weight loss) and 0.86 for Al_C and Al_E respectively. Moreover, the oxidation of Al_C flaky powder into alumina takes place in the range 300–600 °C, in the solid state and then at $T > 660$ °C, in the liquid phase, whereas Al_E globular powder is primarily oxidised at $T > 660$ °C, i.e in the liquid phase. As the theoretical relative weight gain for a full oxidation of the aluminium through the reaction:

$$4/3Al + O_2 = 2/3[Al_2O_3]$$

is $\Delta m/m_0 = 0.89$, it appears, from the previous results, that the Al_C metal surfaces seem initially to be more oxidised than the Al_E ones. The difference in morphology between the Al_C and Al_E particles can explain this

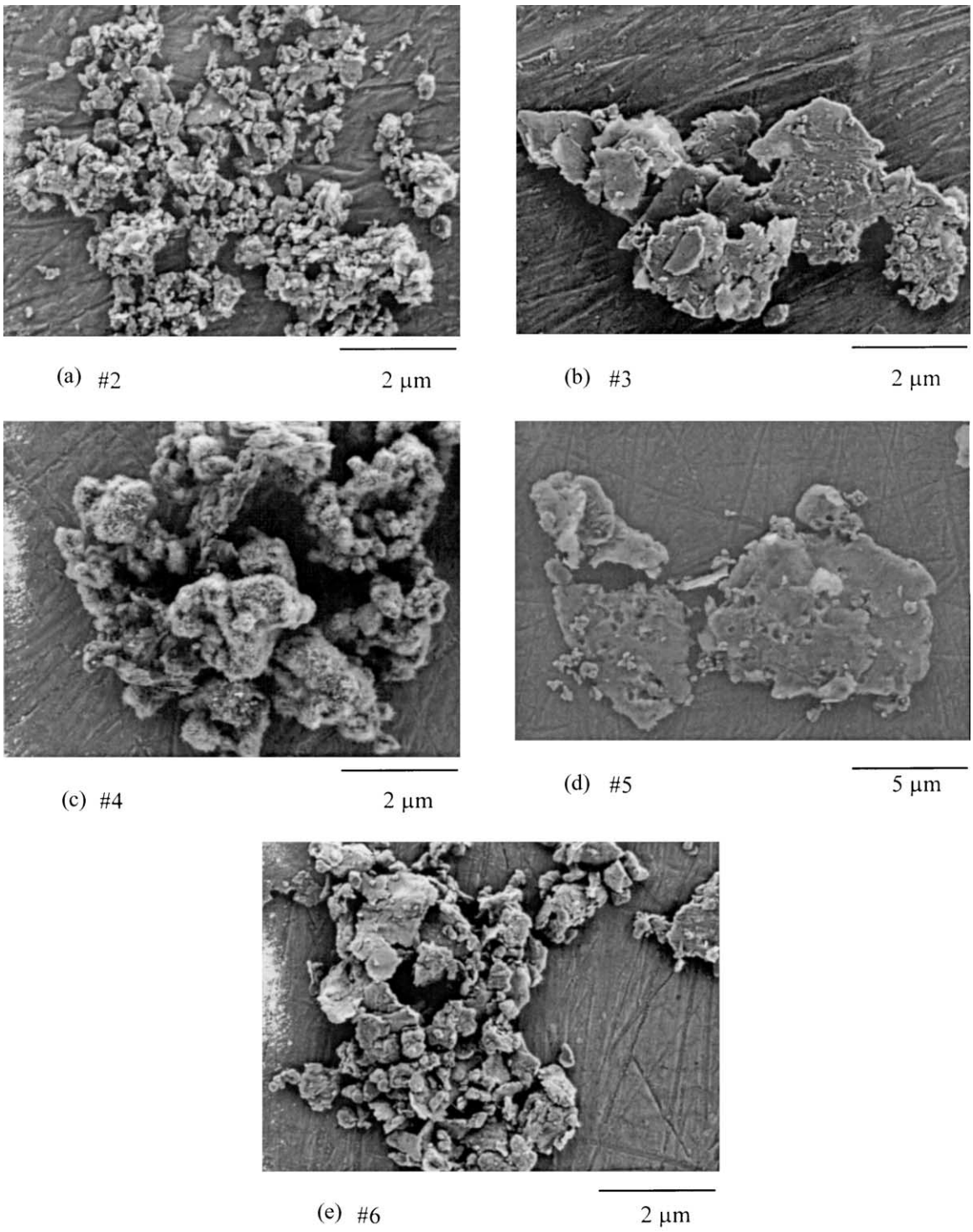

Fig. 3. SEM of powder mixtures after attrition milling.

phenomenon, but especially the specific area values of the Al powders. Indeed, it seems normal that the Al_2O_3 oxide layer formed by surface contact with air is more important for the Al_C particles, with the higher specific area than for the Al_E powder. So, the oxidation potential during reaction-bonding for Al_C particles should be lower than for Al_E powder. This difference of the specific area values is also responsible for the oxidation behaviour of the two aluminium raw materials. Indeed, the high specific area of the Al_C particles permits an increase of aluminium oxidation in the solid state. Finally, between room temperature and $\sim$300 °C, the weight loss reveals the evaporation of fugitive species (such as H_2O).

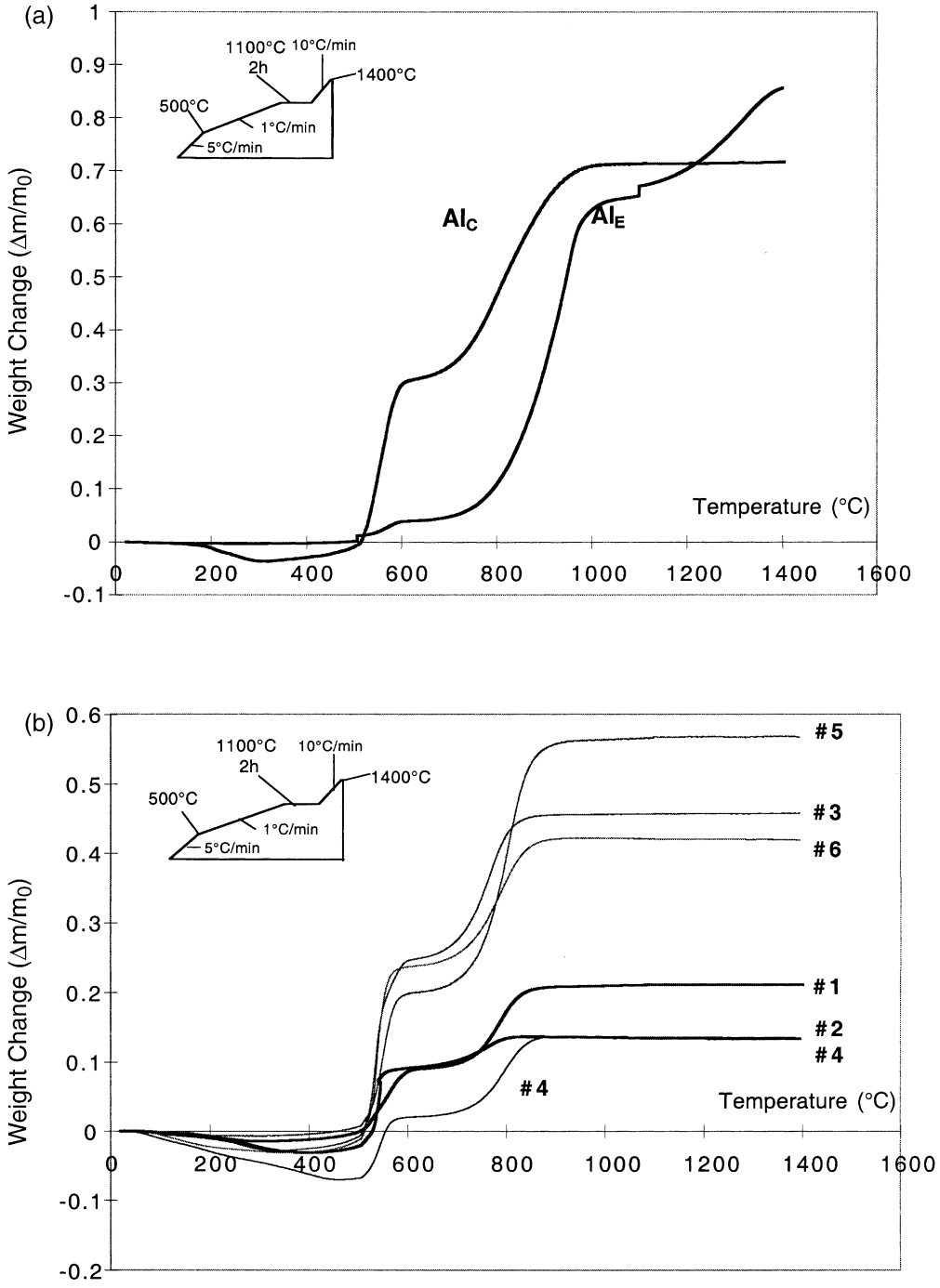

Fig. 4. Weight changes of Al powders (a) and powder mixtures (b).

For all the TGA curves of the powder mixtures (Fig. 4b), the oxidation rate is first very high, but at about 580 °C it slows down and increases again above the melting temperature of Al, until at about 900–1000 °C oxidation is complete. According to these curves the aluminium, in the milled powder mixtures, is oxidised through solid-gas and liquid-gas reactions. In particular, whereas the raw Al_E globular aluminium has shown principally an oxidation step in the liquid state (Fig. 4a), the batches #4–#6, exhibiting similar comminution of the Al_E particles, are now oxidised both in the solid and liquid states. It is interesting to note that, when milling time increases, for the same composition of RBAO mixture, the fraction of Al oxidised below the melting temperature of Al increases strongly (comparison of batches #5 and #6). The attrition milling of the Al_E particles is responsible of this behaviour change. The decrease of the Al_E particle size and the modification of

the shape, during the attrition-milling, contribute to increase the specific area of the milled Al_E powder, and favour the solid/gas oxidation [14].

The reaction-bonding stages observed in the present diagrams correspond to the classical stages of the RBAO process, detailed by Claussen et al. [9]. This TGA behaviour has been more studied and interpreted by Wu et al. [6] who suggest that Al oxidation is controlled by the formation of micro-cracks. In the present work, the most important features that influence the oxidation behaviour of the powder mixtures, are: *(i)* the different oxidation behaviour between the Al_C and Al_E precursor powders due to the difference in shape and granulometry, *(ii)* the fraction of Al oxidised in the raw materials before and after milling and *(iii)* the degree of comminution of the Al powder.

Typical dilatometric curves, up to 1300 °C, are given in Fig. 5. The alumina batch #0 shows any expansion, whereas, due to the oxidation of Al, all the RBAO materials show an expansion step followed by a sintering step. Among the Al_C based RBAO materials, the batches #1 and #2 present two distinct behaviours. For the batch #1 the expansion step is maximum with a corresponding dimension change of about 4%. In this non-milled powder mixture, the proportion of Al_C content which can be oxidised is maximum. For the batch #2 the amount of Al_C oxidised during the milling process is important. Consequently, the volume expansion associated with the oxidation of the aluminium is insufficient to compensate the natural sintering of the formed alumina and the sintering behaviour is similar to that of the reference alumina batch #0. The other attrition-milled materials are characterised by a limited shrinkage and the dimension change that corresponds to the expansion step is lower than to 2%. Table 3 presents the densities and the percentage of the theoretical density (%TD) before and after the dilatometric analysis and the total relative dimension change of the samples. The advantages of the milling process for the Al_E based RBAO mixtures is evidenced by the comparison of the sintering behaviour of the three batches #0, #1 and #5 showing the best sintering behaviour from the same initial relative density (53%). The final densities of these samples are 61%, 64% and 65% corresponding respectively to linear dimensional changes of −5.3%, −0.6% and 1%. For the batch #5, after a short milling time and a small oxidation during milling process, the Al_E globular particles have been laminated into like Al_C flakes of the batch #1 and a low shrinkage behaviour similar to that of the batch #1 is thus obtained.

Table 3
Dilatometric properties

Green parameters		Sintered parameters		Dimensional change	
Batches	Density	%TD	Density	%TD	%
#0	2.09	53	2.43	61	−5.3
#1	1.84	53	2.55	64	−0.6
#2	2.01	56	2.63	66	−5.2
#3	2.00	64	2.55	64	−0.3
#4	1.81	52	2.11	53	−1.7
#5	1.62	53	2.59	65	+1.0
#6	1.87	58	2.60	65	−0.4

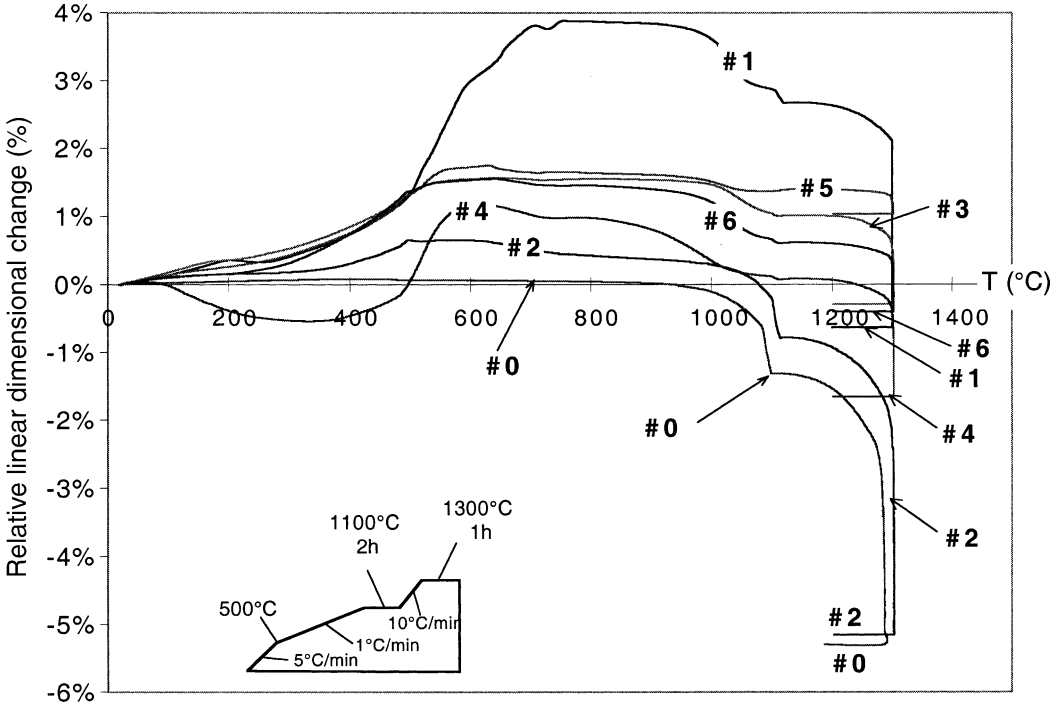

Fig. 5. Dilatometer diagram of dry pressed RBAO discs.

3.3. Microstructure and mechanical properties

The selected RBAO heat-treatment to prepare the three-point bending samples consists of several heating rates (0.25–1 °C/min), with four holds for 1 h up to 1100 °C and a final hold for 3 h at 1250 °C. The holds at 500 and 600 °C promote Al to Al_2O_3 oxidation in the solid state whereas the ones at 700 and 1100 °C complete the oxidation in the liquid phase and the sintering of porous samples . The hold at 1250 °C was to sinter more dense samples. Cooling rate of the cycle was 1 °C/min. The lower heating rate of the cycle (0.25 °C/min) is used between 450 and 1100 °C in order to solve the problem of sample cracking, which is most often encountered at high aluminium contents (>45 vol.%) [7]. Indeed, a recent work [16] has shown that, to avoid sample cracking, the heating rate in the temperature range of 450–600 °C should be reduced to ⩽1 °C/min. The maximum sintering temperature during the last hold was deliberately chosen ⩽1250 °C. Indeed, one of the possible applications of the RBAO ceramics is the processing of oxide/oxide composites, as Nextel/Al_2O_3 composites. However, the thermal stability of the Nextel fibres is limited: for example, the use temperature of the Nextel 720 fibre is 1204 °C [17]. That's why, to process Nextel/RBAO composites, the sintering treatment of the RBAO matrix will not exceed 1200–1250 °C.

The RBAO sample obtained from the batch #2 sintered at 1250 °C shows an homogeneous microstructure, with a fine alumina grain size (Fig. 6a). The large fragmentation of the Al_c particles and the de-agglomeration of the powder mixture (Al/Al_2O_3 volume ratio: 40/60) permits to obtain a sample with a very small grain size. The RBAO sample obtained from the batch #4 (Al/Al_2O_3 volume ratio: 60/40) sintered at 1100 °C is also characterised by rather equiaxed and fine alumina grains (Fig. 6b). Here again, this is the result of the fragmentation of the Al_E particles of the mixture during the milling process. Finally, the microstructure of the RBAO sample obtained from the batch #6 (Al/Al_2O_3 volume ratio: 80/20) sintered at 1250 °C reflects the specific morphology produced by a large fragmentation of the Al_E particles of the powder mixture. Small equiaxed alumina grains are observed as well as small alumina grains with a rather flake shape (Fig. 6c).

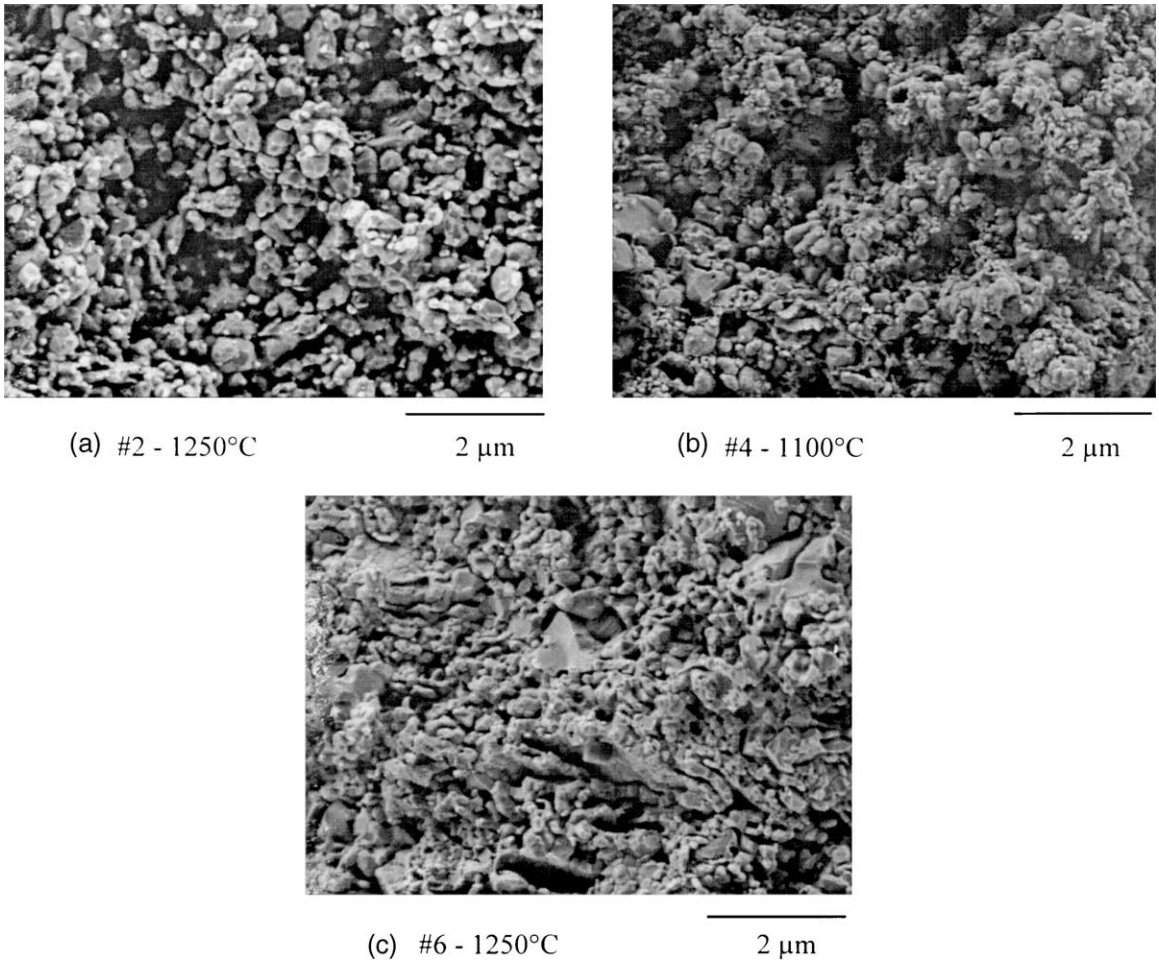

Fig. 6. SEM of the sintered RBAO ceramics.

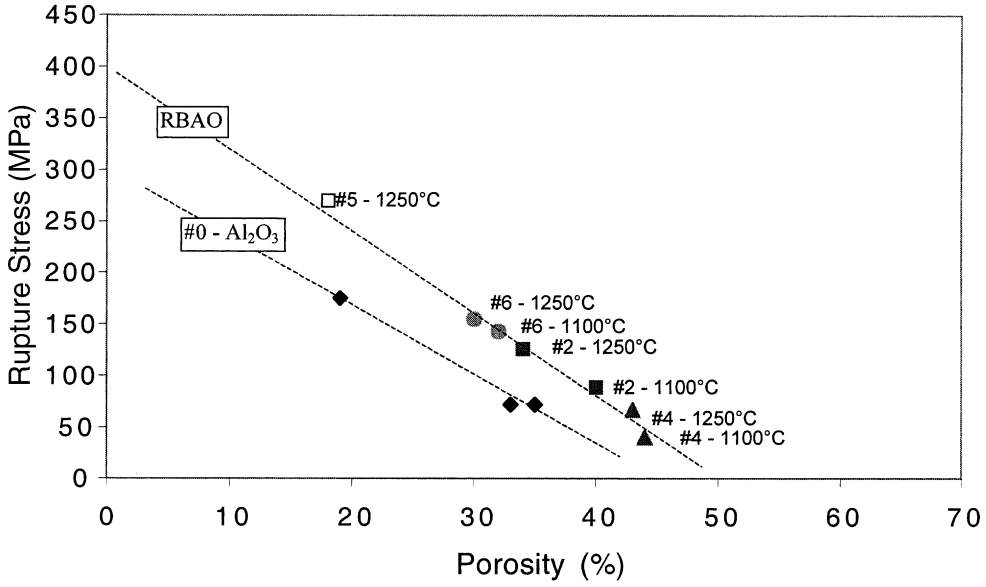

Fig. 7. Bending strengths of RBAO and conventional Al_2O_3 ceramics.

The bending strength of porous RBAO samples (batches #2, 4, 5, 6), together with that of conventional [18] porous Al_2O_3 (batch #0) is presented in Fig. 7, as a function of the porosity. The strength of RBAO material is superior to that of conventional alumina one over the whole porosity range. It has been already seen that at a given porosity the strength of RBAO ceramics is much higher than that of conventional Al_2O_3. The mechanical strength measured in the present is in agreement with those reported by. Claussen et al. [14] and by Luyten et al. [19] for a similar RBAO system. It is generally supposed that this behaviour had something to do with the special microstructure of RBAO ceramics [6,9,20]. Usually, we can consider the influence of microstructure on the strength of ceramics in terms of the key variables of the simple Griffith approach of the fracture mechanics: i.e., the critical flaw size c and the effective surface energy γ_i for the initiation of fracture under the fracture stress $\sigma_f = Y(2E\gamma_i/c)^{1/2}$. Intuitively the flaw size is related to the grain size or to the pore size. The main conclusion concerning the relation between flaw size and microstructure is that the flaw size approximates to the largest grain size or to the largest pore of the microstructure. Thus for some authors, the surprising improved mechanical strength observed can be explained by the mechanism of neck forming during the oxidation and sintering of the RBAO process [4,21]. In these porous RBAO samples the mechanism of neck forming should be controlled by the special and homogeneous microstructure observed: big original Al_2O_3 grains, surrounded by smaller grains, coming from oxidised Al [22]. However, as shown above, it is the largest grain size of the microstructure that is pertinent. In our case, the improved mechanical strength observed cannot be justified by this flaw size argument because the grain size of the conventional alumina is not the largest. The factors controlling surface energy, as the chemistry of grain boundary, can thus be put forward to account for the improve of the strength in RBAO samples. Due to the use of Al metal in the RBAO process, the amount of impurity present in the materials is more important in RBAO samples than in conventional alumina and the chemical nature of the grain boundaries will change from RBAO samples to conventional alumina. The possibility of a stronger atomic bonding which should increase the fracture resistance of alumina interfaces in doped alumina has already been discussed by Wang and Raj [23]. Like in metals, where segregation reduces the grain boundary energy γ_b [24], it can be expected that strong segregants change the surface energies in RBAO ceramics. If impurity atoms prefer to reside on a grain boundary rather than on a free surface, thus segregated atoms do not affect solely the free surface energy. In this situation the reduction of the grain boundary energy implies an increase of the work of fracture of a grain boundary $2\gamma = 2\gamma_s - \gamma_b$, and this means a stronger cohesive strength.

4. Conclusions

Reaction-bonded Al_2O_3 (RBAO) ceramics were fabricated from attrition-milled Al/Al_2O_3 powder mixtures. Two different Al precursor powders were employed and several contents of Al were used. The final powder morphology which depends directly on the characteristics of the raw materials and the attrition-milling conditions

determines the microstructural characteristics of the sintered RBAO ceramics.

Among the important processing parameters [16,25], the milling conditions, and the temperature holds in the heating cycle have been studied. Generally, after a milling time of about 8–14 h the two types of precursor powders tend to exhibit less different morphologies and this time was sufficient to reduce Al mean particle sizes to about ~1 μm in order to have sintering with low dimension variation.

In the present work, it was demonstrated that RBAO ceramics can be processed, at low temperature (1100–1250 °C) with good mechanical properties: ~270 MPa at ~80% TD for the RBAO ceramic, against ~175 MPa at ~80% TD for a conventional alumina.

The improved mechanical strength observed cannot be justified alone by a flaw size argument because the grain size of the conventional alumina was not the largest. The factors controlling surface energy, as the chemistry of grain boundary, can thus be put forward to account for the improve of the strength in RBAO samples.

Acknowledgements

The authors wish to thank J.F. Justin, A. Vallejo and M.H. Ritti, from ONERA-DMSC, for their help in mechanical tests, TGA/DTA measurements and SEM observations, respectively.

References

[1] W.E. Washburn, W.S. Coblenz, Reaction-formed ceramics, Am. Ceram. Soc. Bull. 67 (1988) 356–360.
[2] Y. Chiang, J.S. Haggerty, R.P. Messner, C. Demetry, Reaction-based processing methods for ceramic-matrix composites, Am. Ceram. Soc. Bull. 68 (1989) 420–425.
[3] A.J. Moulson, Review—reaction-bonded silicon nitride: its formation and properties, J. Mater. Sci. 14 (1979) 1017–1051.
[4] N. Claussen, T. Le, S. Wu, Low-shrinkage reaction-bonded alumina, J. Eur. Ceram. Soc. 5 (1989) 29–35.
[5] S. Wu, N. Claussen, Fabrication and properties of low-shrinkage reaction-bonded mullite, J. Am. Ceram. Soc. 74 (1991) 2460–2463.
[6] S. Wu, D. Holz, N. Claussen, Mechanisms and kinetics of reaction-bonded aluminum oxide ceramics, J. Am. Ceram. Soc. 76 (1993) 970–980.
[7] D. Holz, S. Wu, S. Scheppokat, N. Claussen, Effect of processing parameters on phase and microstructure evolution in RBAO ceramics, J. Am. Ceram. Soc. 77 (1994) 2509–2517.
[8] D. Holz, N. Claussen, Reaction bonded Al_2O_3 (RBAO) and related technology, Ceram. Eng. Sci. Proc. 16 (1995) 252–258.
[9] N. Claussen, N.A. Travitzky, S. Wu, Tailoring of reaction-bonded Al_2O_3 (RBAO) ceramics, Ceram. Eng. Sci. Proc. 11 (1990) 806–820.
[10] F.F. Lange, M.M. Hirlinger, Hindrance of grain growth in Al_2O_3 by ZrO_2 inclusions, J. Am. Ceram. Soc. 67 (1984) 164–168.
[11] J. Wang, R. Stevens, Review—zirconia toughened alumina (ZTA) ceramics, J. Mater. Sci. 24 (1989) 3421–3440.
[12] D. Holz, M. Roger, R. Janssen, N. Claussen, Mechanical properties of reaction bonded Al_2O_3/ZrO_2 composites, Ceram. Eng. Sci. Proc. 15 (1994) 651–658.
[13] A.G. Gesing, G. Burger, E. Luce, N. Claussen, S. Wu, N.A. Travitzky, Preparation and characterization of reaction-bonded aluminum oxide (RBAO) matrix SiC particulate filler composites, Ceram. Eng. Sci. Proc. 11 (1990) 821–841.
[14] N. Claussen, R. Janssen, D. Holz, Reaction-bonding of aluminum oxide (RBAO) — science and technology, J. Ceram. Soc. Jpn 103 (1995) 738–746.
[15] N. Claussen, S. Wu, D. Holz, Reaction bonding of aluminum oxide (RBAO) composites: processing, reaction mechanisms and properties, J. Eur. Ceram. Soc. 14 (1994) 97–109.
[16] S.P. Gaus, M.P. Harmer, H.M. Chan, H.S. Caram, Controlled firing of reaction-bonded aluminum oxide (RBAO) ceramics: Part I, continuum-model predictions, J. Am. Ceram. Soc. 82 (1999) 897–908.
[17] 3M company, Nextel ceramic fiber typical properties (private communication).
[18] S. Bertrand, Internal report of ONERA-DMSC (private communication).
[19] J. Luyten, J. Cooymans, P. Diels, J. Sleurs, The effect of powder conditioning on the synthesis of RBAO, Silicates Industriels 7–8 (1992) 91–94.
[20] J. Luyten, J. Cooymans, R. Leysen. Shaping of a RBAO-membrane support, in: Euro-Ceramics V, Key Engineering Materials, Vols. 132–136, 1691–1694, Trans Tech Publications, Switzerland, 1997.
[21] J. Luyten, J. Cooymans, P. Diels, J. Sleurs, RBAO-used as part of a membrane configuration, in: P. Duran, J.F. Fernandez (Eds.), Third Euro-Ceramics V. 1, Faenza Ed Iberica SL, Madrid, 1993.
[22] J. Luyten, J. Cooymans, C. Smolder, S. Vercauteren, E.F. Vansant, R. Leysen, Shaping of multilayer ceramic membranesby dip coating, J. Eur. Ceram. Soc. 17 (1997) 273–279.
[23] J. Wang, R. Raj, Estimate of the activation energies for boundary diffusion from rate-controlled sintering of pure alumina, and alumina doped with zirconia or titania, J. Am. Ceram. Soc. 73 (1990) 1172–1175.
[24] D. Gupta, Influence of solute segregation on grain-boundary energy and self diffusion, Metall. Trans. A 8A (1977) 1431–1438.
[25] S.P. Gaus, P.M. Sheedy, H.S. Caram, H.M. Chan, M.P. Harmer, Controlled firing of reaction-bonded aluminum oxide (RBAO) ceramics: Part II, experimental results, J. Am. Ceram. Soc. 82 (1999) 909–915.